Supplementary Information

for

Visualization of UV-A light-induced damage to plasma membranes of eye lens

Peter S. Sherin,[1,2*] Aurimas Vysniauskas,[3,4] Ismael López-Duarte,[1] Peter R. Ogilby,[5] Marina K. Kuimova[1*]

[1] Chemistry Department, Molecular Sciences Research Hub, Imperial College London, 82 Wood Lane, London, W12 0BZ, UK

[2] International Tomography Center SB RAS, Institutskaya street 3A, Novosibirsk, 630090, Russia

[3] Center for Physical Sciences and Technology, Saulėtekio av. 3, Vilnius, LT-10257, Lithuania

[4] Chemistry Department, Vilnius University, Naugarduko st. 24, Vilnius, LT-03225, Lithuania

[5] Department of Chemistry, Aarhus University, Langelandsgade 140, Aarhus, DK-8000, Denmark

*Corresponding authors:

Dr Peter S. Sherin (p.sherin@imperial.ac.uk), Dr Marina K. Kuimova (m.kuimova@imperial.ac.uk)

Table of Content:

Section S1. BODIPY-based rotors

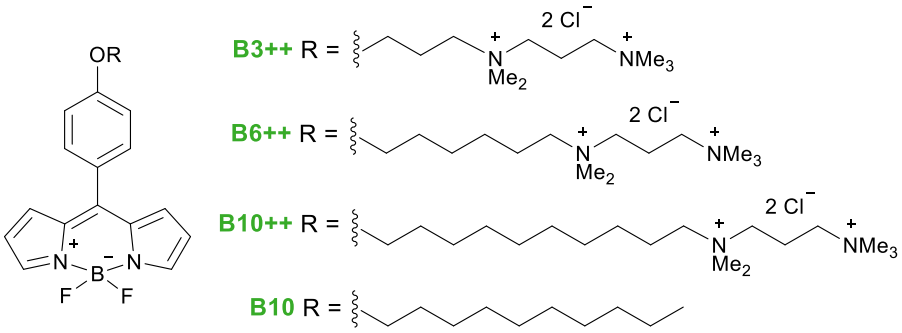

Chart S1. Chemical structures of BODIPY-based rotors.

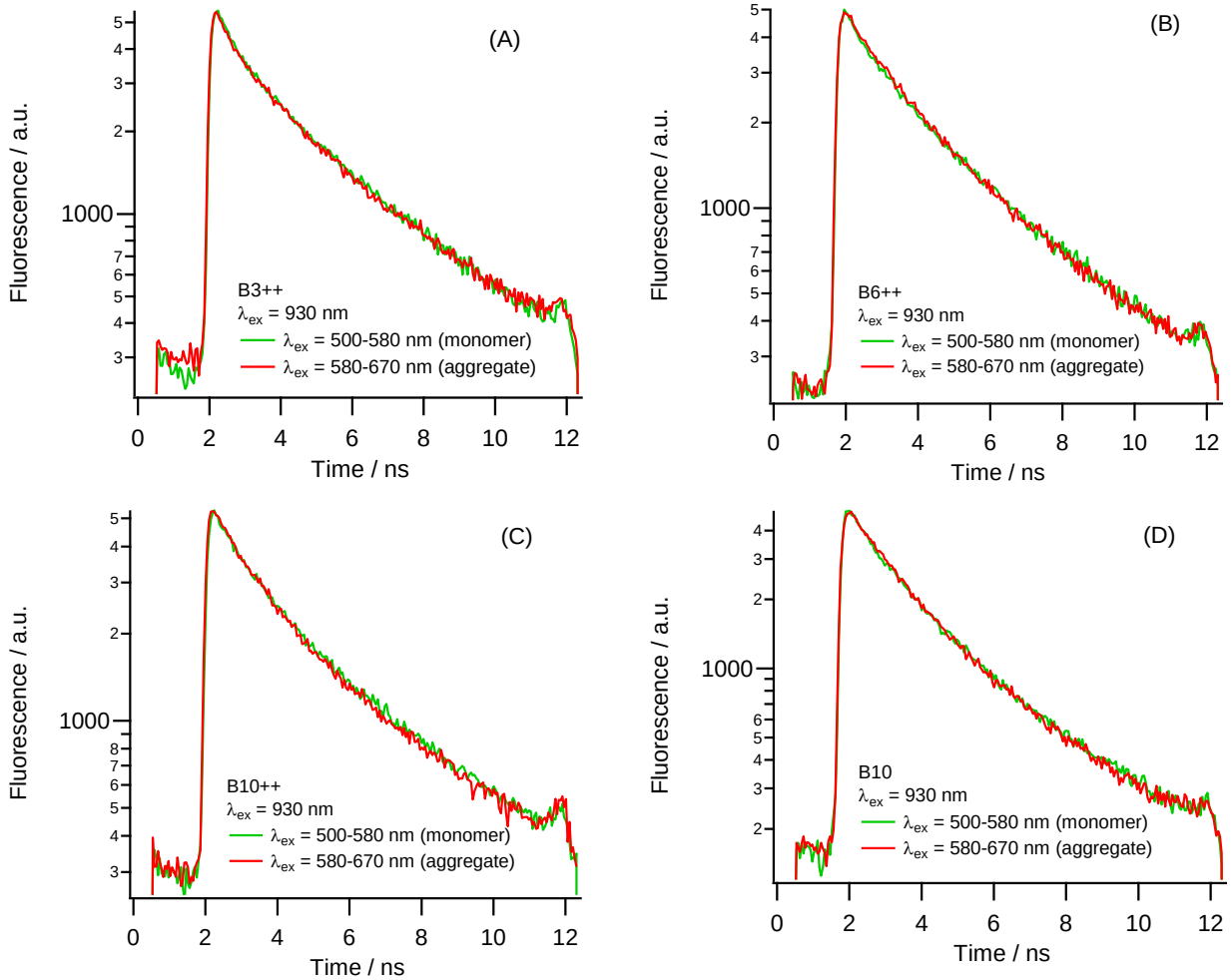

Figure S1. Time resolved fluorescence decays recorded following 930 nm excitation of BODIPY-based molecular rotors within plasma membranes of porcine eye lens: (A) **B3++**, (B) **B6++**, (C) **B10++**, (D) **B10**. Eye lens slices were stained with dyes with concentrations of 10 μM according to the optimized protocol (see methods, main text).

The aggregation of a BODIPY-based rotor manifests itself by the appearance of a longer decay component, which is particularly noticeable in the spectral windows 590-670 nm, corresponding to the aggregated dye as compared to monomers, which mainly emit at 500-580 nm [1]. Figure S1 demonstrates the coincidence of fluorescence decays recorded in two spectral windows corresponding to monomers (500-580 nm) and aggregates (590-670 nm) for all BODIPY-based rotors used in this work within membranes of eye lenses.

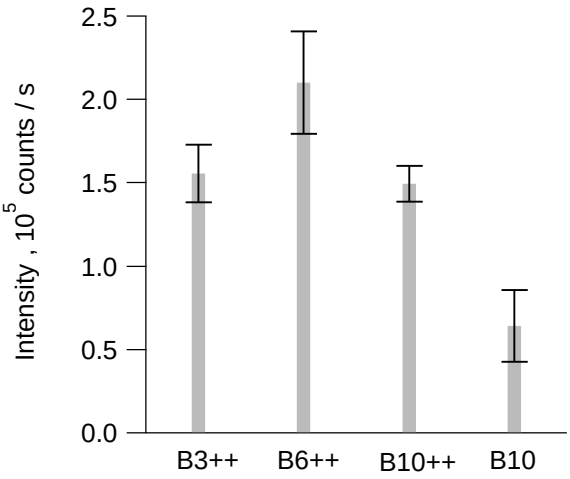

Figure S2. Fluorescence signal intensities recorded using different BODIPY-based rotors within eye lens membranes measured under 930 nm irradiation with the average power of 0.45 mW at the output of x100 objective. All dyes in concentrations 10 μM were incubated with eye lens slices for 10 mins (see details in Experimental section of the main text).

Lifetime data analysis.

BODIPY-based rotors within plasma membranes of eye lens exhibit long decays exceeding the time frame available for measurements (12.5 ns due to laser repetition rate of 80 MHz). This leads to an incomplete decay (manifested by a non-flat baseline in pre-pulse regions, e.g. in Figure S2 and Figures 1 and 3 of the main text). This could be accounted for by the corresponding fitting model in SPCImage software (incomplete decay).

The critical parameter for this kind of analysis is the background noise during the signal acquisition. The contribution of this noise could be estimated from the Instrument Response Function (IRF) time profile. This fitting option is available in an alternative software package, FLIMfit (termed 'pre-pulsing' in FLIMfit). Taking pre-pulsing into account led to a small shift of resulting lifetime distributions by 30-50 ps to lower values. The fixation of background noise at zero value gave the identical distributions of lifetimes from both software packages, SPCImage and FLIMfit. However, SPCImage is more useful for the fitting of large volumes of data, therefore, all presented data were analysed with SPCImage using the model of incomplete decay with offset values set to zero.

According to calibration curve (Figure S3 of SI), the measured values $\tau_1 = 0.97 \pm 0.09$ ns and $\tau_2 = 4.22 \pm 0.20$ ns could be converted to viscosities $\eta_1 = 44 \pm 7$ cP and $\eta_2 = 580 \pm 50$ cP. Though the η_1 value well agrees with the value *ca* 50 cP reported in our previous work [2], the η_2 value is significantly lower than the earlier reported value with **B3+**, Figure S3. This discrepancy could be due to several factors:

- Different origin and size of lens samples. A direct comparison of eye lenses used in this work (abattoir near Bedford, UK) with one used in previous work (abattoir near Novosibirsk, Russia) has shown a distinct variation in their sizes; for instance, the diameters of lenses were 10 and 12 mm, respectively (Figure S4 of SI). This difference may originate from the pig breed, seasonal changes in nutrition, etc.
- Type II oxidation leading to viscosity increase may have occurred in our previous work [2], due to excessive irradiation of the sample
- Improved lifetime/viscosity calibration curves for **B6++** and **B3+**

Additional studies are required to examine these factors affecting the eye lens membrane structure, which are out of the scope of this present paper. In this work we used eye lens collected in a short period (September-October 2020, N = 24) with diameters of 10 ± 1 mm, masses 410 ± 25 mg and showed very similar lifetimes for **B6++**. To avoid contradictions with previously reported viscosities, in this work we compare only the lifetimes without conversion to the absolute viscosity values.

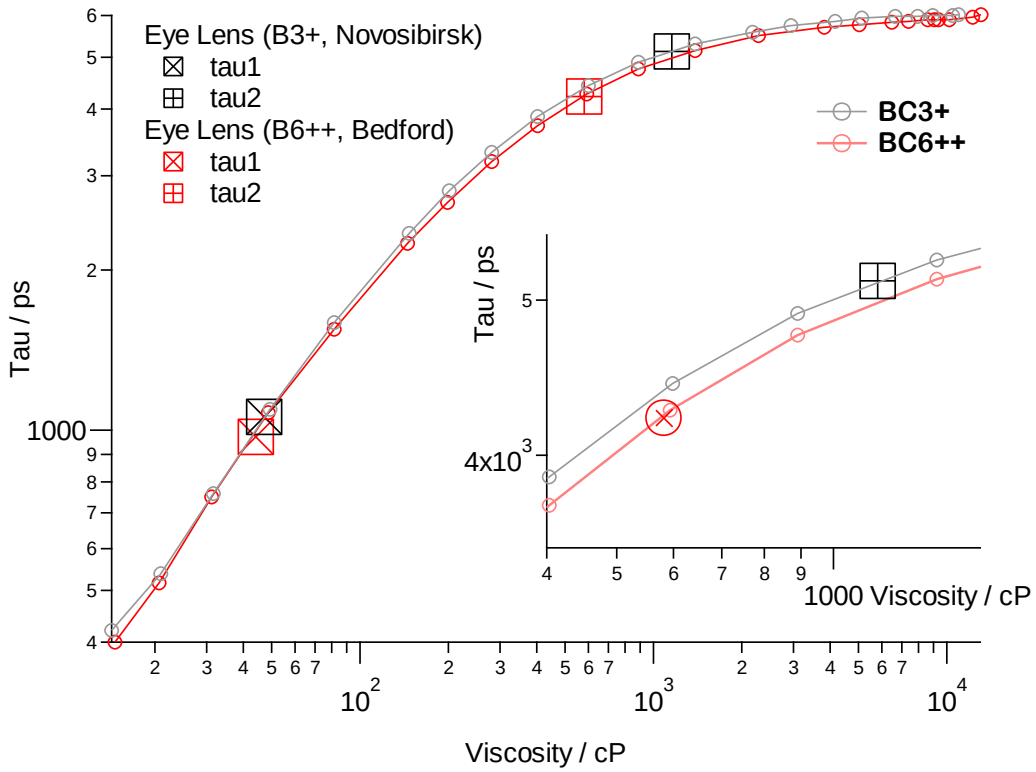

Figure S3. Lifetime/viscosity calibration curves recorded for **B3+** and **B6++** in pure glycerol at different temperatures (all data recorded in this work). The eye lens lifetimes for both dyes are also shown (data for **B3+** taken from [2] and for **B6++** from this work). Inset: the zoom in of same data for the region of high viscosities (400 – 1600 cP).

Section S2. Porcine eye lenses

Figure S4. Frozen eye lenses from Novosibirsk (Russia) and Bedford (UK). Photo was made in cryotome at -20C.

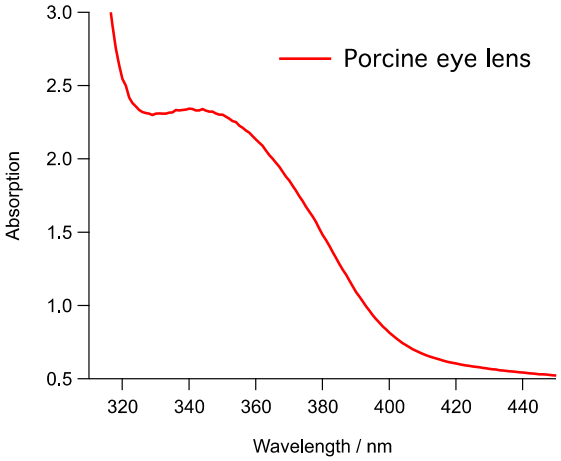

Figure S5. Absorption spectrum of the whole porcine eye lens immersed in AHA in 1 cm pathlength quartz cell.

Section S3. Measurements of quantum yields of singlet oxygen for BODIPY-based rotors.

For singlet oxygen measurements we chose **BH** and **B10** (see chemical structures below) as close analogues of **B6++** with good solubility in all organic solvents including non-polar solvents. **B6++** due to the presence of charged groups is almost insoluble in nonpolar and low polarity solvents.

BODIPY-H (BH) **BODIPY-C10 (B10)**

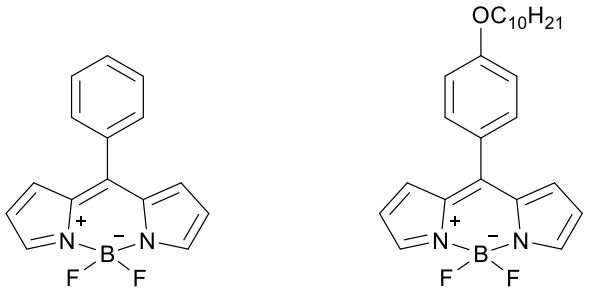

Table S1. Quantum yields of singlet oxygen production for BH and B10 in various solvents.

Solvent properties	Solvent, air saturated	ϕ_Δ		Solvent, oxygen saturated	ϕ_Δ	
		BH	B10		BH	B10
Low ε	Toluene	0.006 ± 0.001	0.010 ± 0.001	Toluene	0.012 ± 0.001	0.021 ± 0.001
High ε	MeOH	0.004 ± 0.001	0.008 ± 0.001	MeOH	0.007 ± 0.002	0.013 ± 0.003
High η	70% G-M*	0.003 ± 0.001	0.006 ± 0.001	–	–	–

*Mixture of 70% Glycerol / 30% MeOH (v/v).

Section S4. Type I photodamage within eye lens membranes

KNA in triplet state readily reacts with tryptophan (Trp) and tyrosine (Tyr) residues via Proton-Coupled Electron Transfer (PCET) [3] and H-transfer [4]. The quenching rate constants for Trp and O_2 are almost the same, 2.5×10^9 $M^{-1}s^{-1}$ [5]; reaction with Tyr is slower, 8.8×10^8 $M^{-1}s^{-1}$ [4]. A lens contains high concentration of proteins, up to 400 mg/ml [6] or approximately 20 mM of monomeric subunits. The total number of Trp and Tyr residues in crystallins (lens proteins) could be estimated as 5% of total number of amino acids (data from Uniprot database, www.uniprot.org). Therefore, the efficient concentrations of both Trp and Tyr could be estimated as 1 mM. Under our experimental conditions the oxygen could not be completely removed from a slice, which was saturated by ambient air. Assuming that oxygen solubility is the lens is the same as in water (50% of wet weight of lens is water), i.e. 20% of 1.4 mM (maximum oxygen solubility in water) that equals 0.28 mM within tissue slice. Thus, the concentration of Type I quenchers (Trp and Tyr) is four times higher than Type II quenchers (O_2). Thus, Type I photodamage is expected to dominate under our experimental conditions.

Section S5. FLIM data

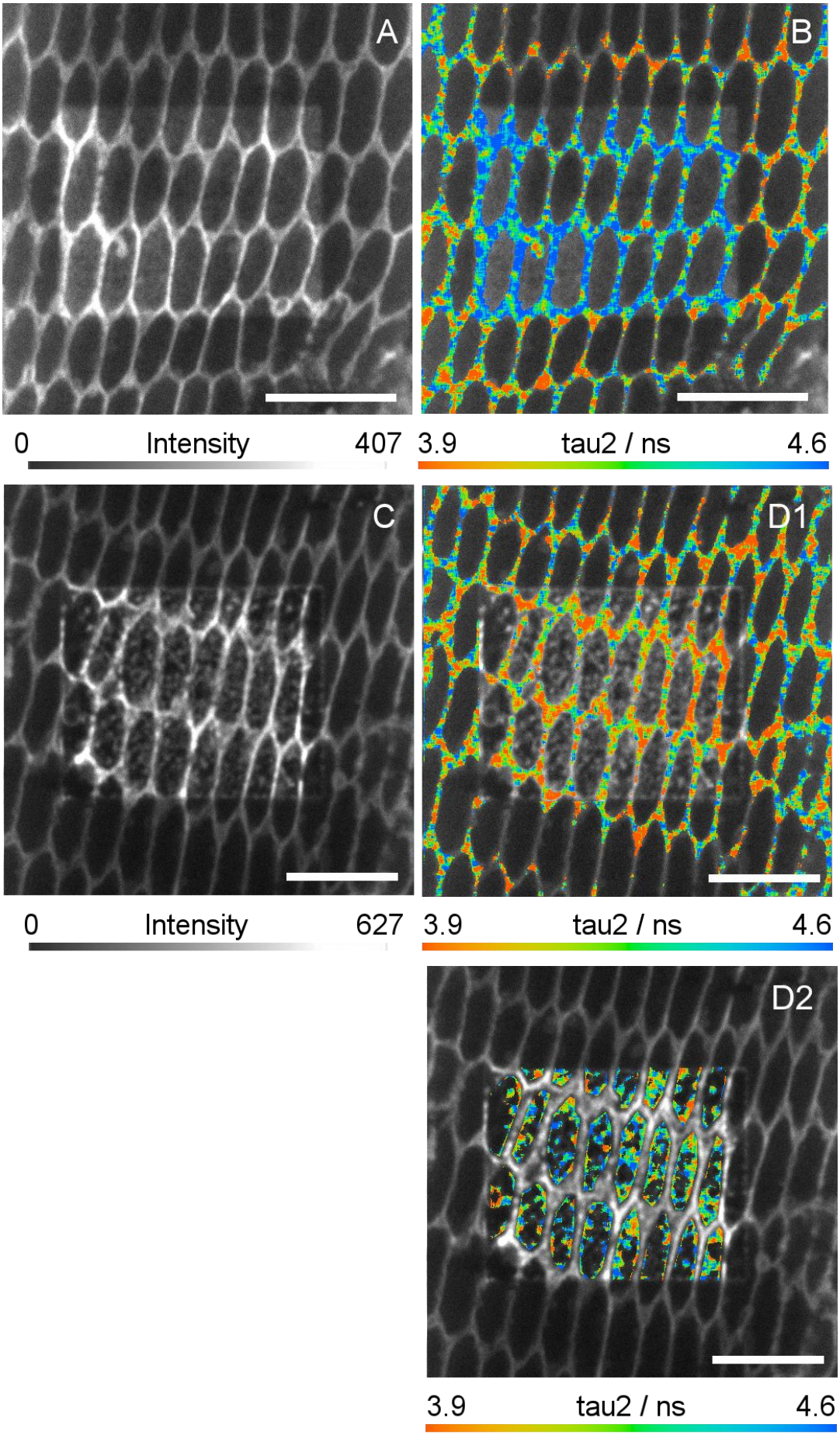

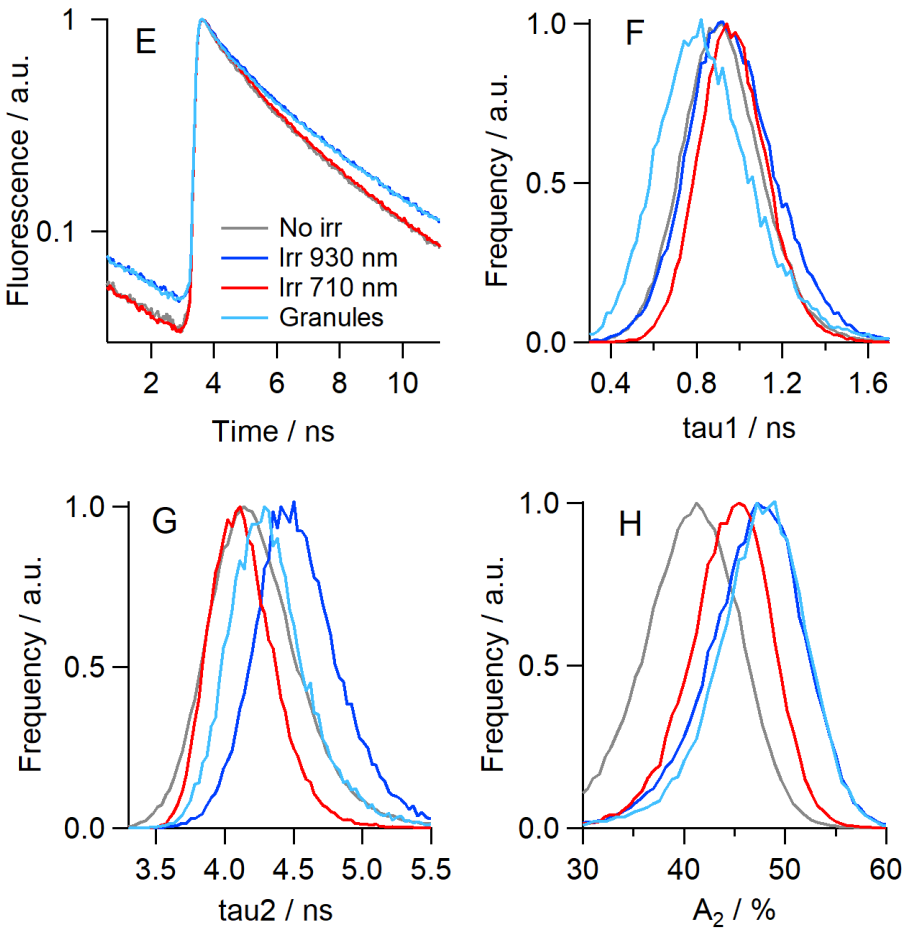

Figure S6. (A, C) Intensity and (B, D) FLIM images of porcine eye lens stained with 10 μM **B6++** following (A, B) 930 nm irradiation or (C, D1, D2) in the presence of 3 mM KNA following 710 nm irradiation (D1 – plasma membranes, D2 – intracellular 'granules'). The central frame was irradiated for 1400 sec at 2.0 mW power at the wavelength indicated, the whole image acquisition time was 300 sec at 0.45 mW. Scale bars are 10 μm. (E-H) FLIM analysis of the data. (E) Averaged time-resolved decays recorded for **B6++** from randomly selected plasma membrane locations. Distributions of τ_1 (F), τ_2 (G) and A_2 (H) obtained from biexponential fits of FLIM data. No irradiation (grey curves), 930 nm irradiation (red curves) and 710 nm irradiation in the presence of KNA (blue curves – plasma membranes, light blue curves – intracellular 'granules'). Independent biological experiments were performed in triplicate, two image frames were analysed per experiment.

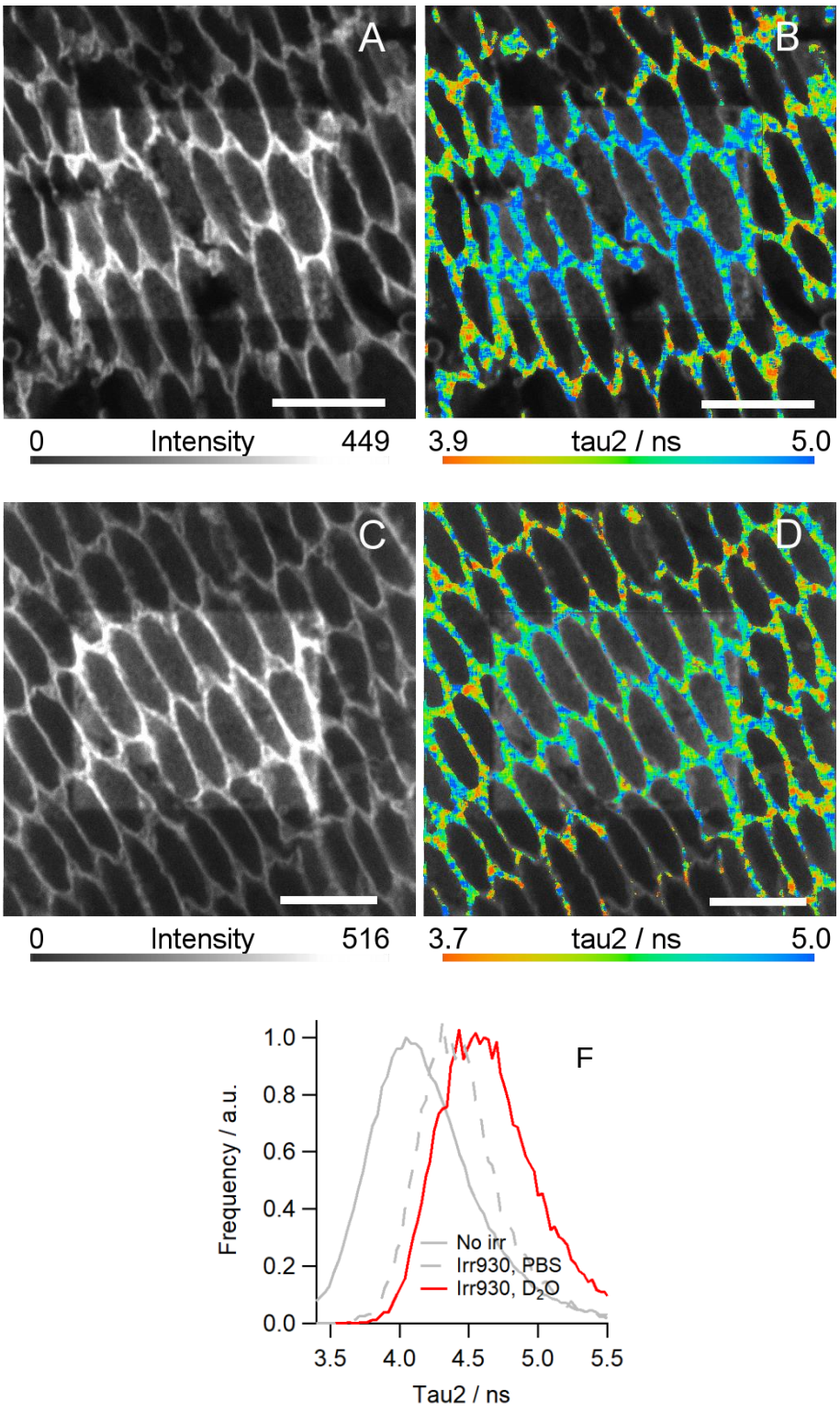

Figure S7. Intensity (A, C) and FLIM (B, D) images of porcine eye lens stained with 10 μM **B6++** in (A,B) D_2O/PBS (9/1 v/v) and (C,D) H_2O/PBS (9/1 v/v) following 930 nm irradiation. The central frame was irradiated for 1000 sec (at 2.0 mW power) at the wavelength indicated, the whole image acquisition time was 300 sec (at 0.45 mW). Scale bars are 10 μm. Both control experiments show a lifetime increase in the irradiated frame (blue colour) with more pronounced effect in the case of D_2O. Independent biological experiments in duplicate, two image frames per experiment. (F) Distributions of τ_2 obtained from biexponential fits of FLIM data: before (solid grey) and after (dashed grey lines) photolysis at 930 nm in the absence and presence of D_2O (red lines).

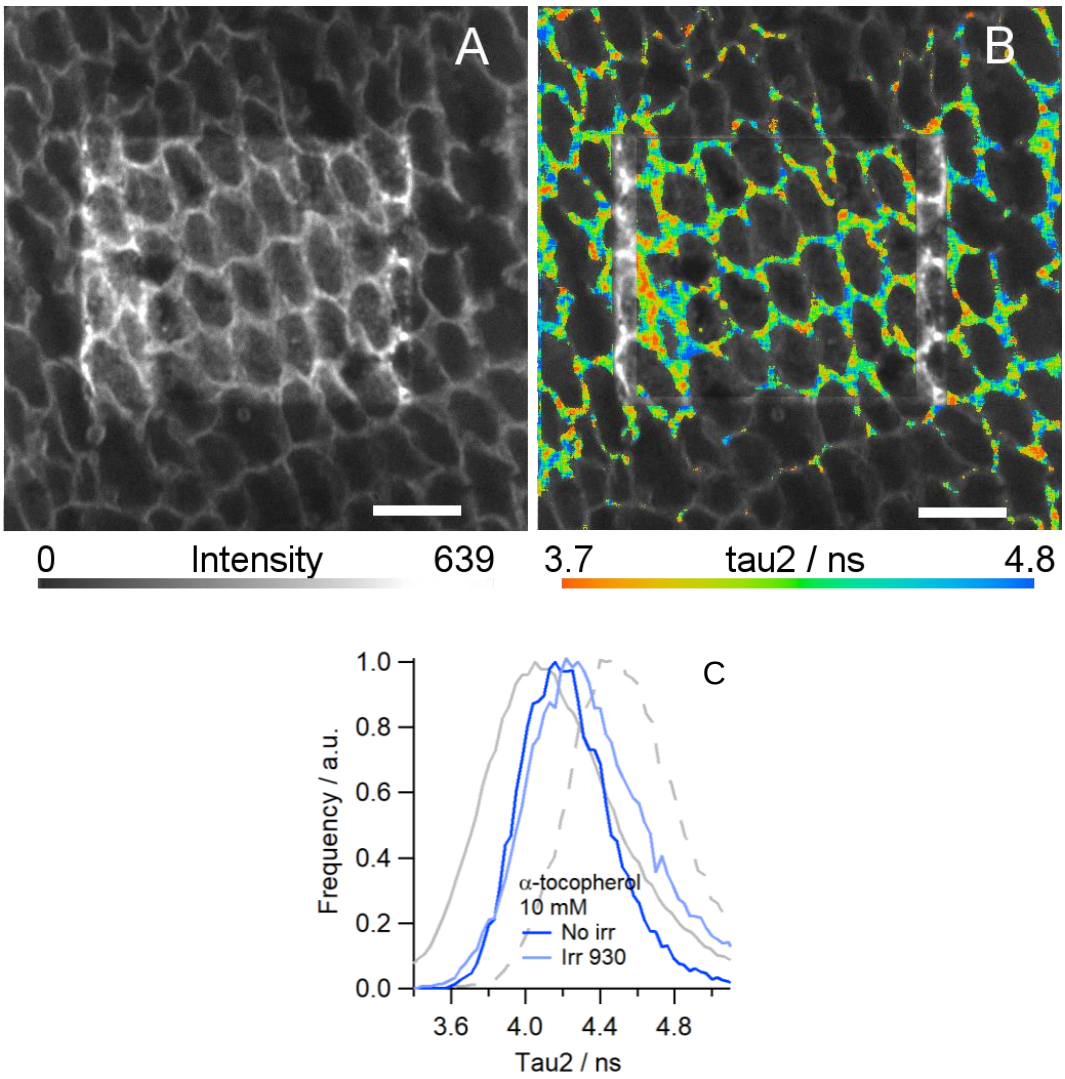

Figure S8. Intensity (A) and FLIM (B) images of porcine eye lens stained with 10 μM **B6++** and 10 μM α-tocopherol in PBS following 930 nm irradiation. The central frame was irradiated for 1400 sec (at 2.0 mW power) at the wavelength indicated, the whole image acquisition time was 300 sec (at 0.45 mW). Scale bars are 10 μm. Minor changes of lifetime (τ_2) in the irradiated frame indicates significant suppression of Type II damage via singlet oxygen by α-tocopherol. Independent biological experiments in duplicate, two image frames per experiment. (C) Distributions of τ_2 obtained from biexponential fits of FLIM data: before (solid grey) and after (dashed grey lines) photolysis at 930 nm in the absence and presence of 10 μM of α-tocopherol (blue lines).

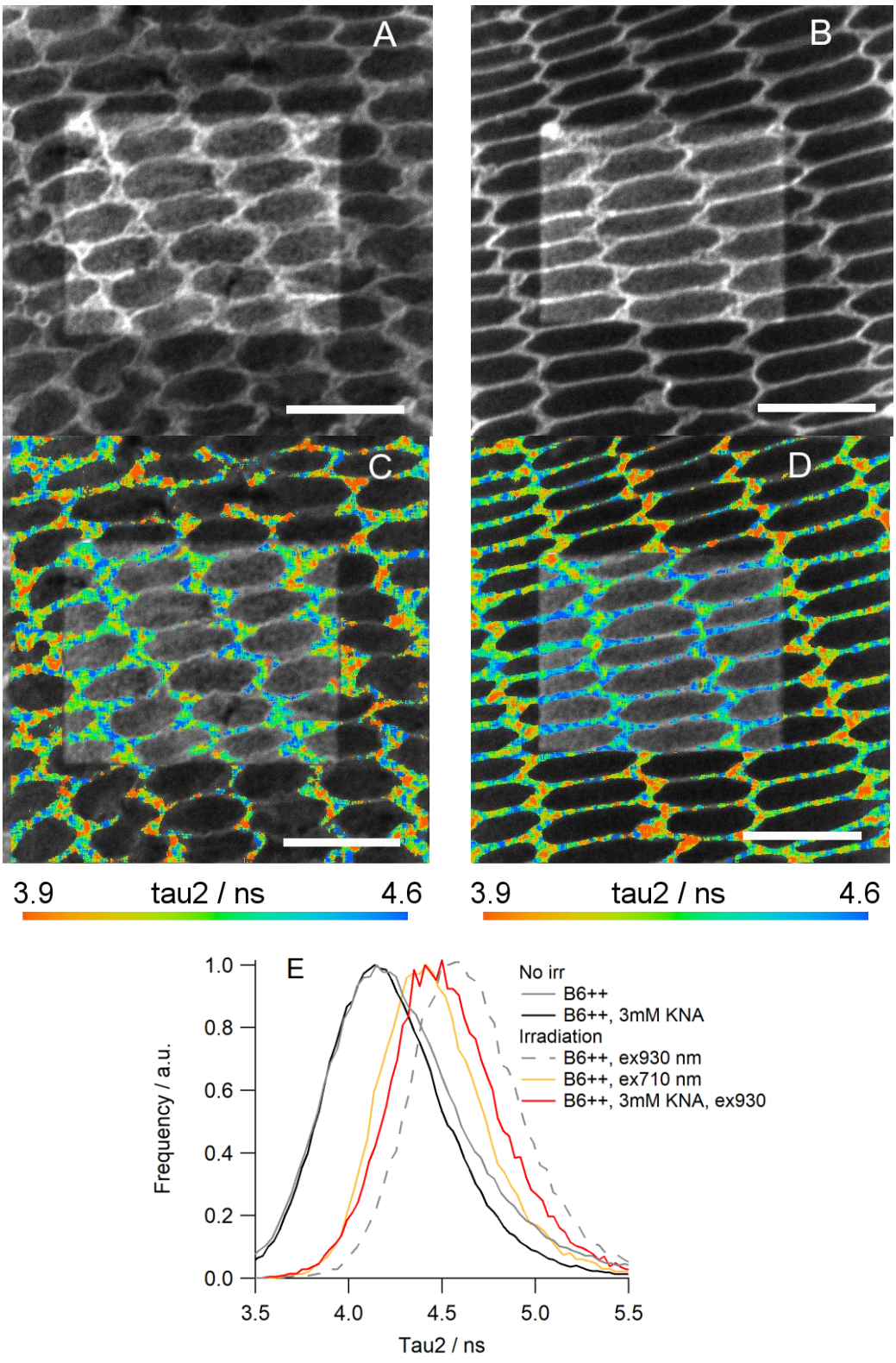

Figure S9. Intensity (A, B) and FLIM (C, D) images of porcine eye lens stained with 10 μM **B6++** following (A, C) 710 nm irradiation in the absence of KNA and (B,D) 930 nm irradiation in the presence of 3 mM KNA. The central frame was irradiated for 1400 sec (at 1.0 mW power) at the wavelength indicated, the whole image acquisition time was 300 sec (at 0.45 mW). Scale bars are 10 μm. Both control experiments show a lifetime increase in the irradiated frame (blue colour). Independent biological experiments in triplicate, two image frames per experiment. (F) Distributions of τ_2 obtained from biexponential fits of FLIM data: before / after photolysis at 930 nm in the absence

(solid / dashed grey lines) and presence (black / red lines) of 3 mM KNA and after photolysis at 710 nm in the absence of KNA (orange line).

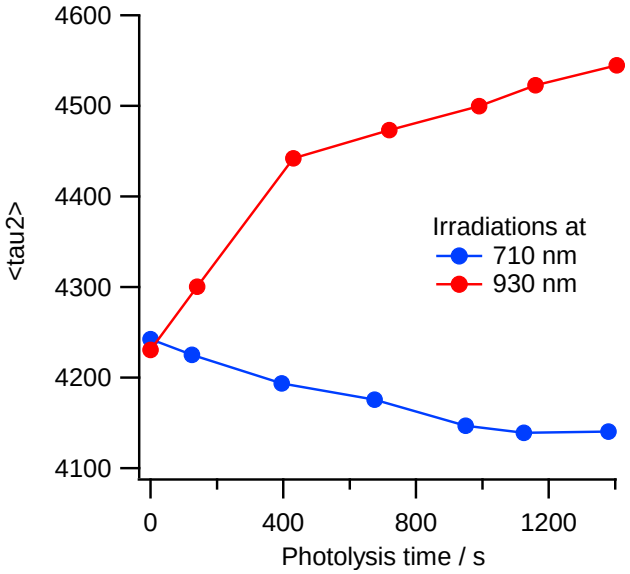

Figure S10. The average value (mass centre of a lifetime distributions) of the longest component (τ_2) of **B6++** decay within plasma membranes of porcine eye lenses during the photolysis of (red) the eye lens slice stained with 10 µM **B6++** at 930 nm and (blue) the eye lens slice stained with 3mM KNA and 10 µM **B6++** at 710 nm. Note that a femtosecond pulsed irradiation from a Ti:Saphire laser at 710 nm could be absorbed in a multiphoton process by both **B6++** and KNA.

References

1. Y. Wu, M. Štefl, A. Olzyńska, M. Hof, G. Yahioglu, P. Yip, D. R. Casey, O. Ces, J. Humpolíčková, M. K. Kuimova, Molecular rheometry: direct determination of viscosity in Lo and Ld lipid phases via fluorescence lifetime imaging Phys. Chem. Chem. Phys. 15 (2013) 14986. https://doi.org/10.1039/c3cp51953h
2. P.S. Sherin, I. Lopez-Duarte, M.R. Dent, M. Kubankova, A. Vysniauskas, J.A. Bull, E.S. Reshetnikova, A.S. Klymchenko, Yu.P. Tsentalovich, M.K. Kuimova, Visualising the membrane viscosity of porcine eye lens cells using molecular rotors, Chem. Sci. 8 (2017) 3523-3528, https://doi.org/10.1039/c6sc05369f
3. Yu.S. Zhuravleva, O.B. Morozova, Yu.P. Tsentalovich, P.S. Sherin, Proton-coupled electron transfer as the mechanism of reaction between triplet state of kynurenic acid and tryptophan, J. Photochem. Photobiol. A.: Chem. 396 (2020) 112522. http://doi.org/10.1016/j.jphotochem.2020.112522.
4. Yu.S. Zhuravleva, Y.P. Tsentalovich, Acid-alkaline properties of triplet state and radical of kynurenic acid, J. Photochem. Photobiol. A: Chem. 365 (2018) 7-12, https://doi.org/10.1016/j.jphotochem.2018.07.029
5. P.S. Sherin, E.A. Zelentsova, E.D. Sormacheva, V.V. Yanshole, T.G. Duzhak, Yu.P. Tsentalovich, Aggregation of α-crystallins in kynurenic acid-sensitized UVA photolysis under anaerobic conditions, Phys. Chem. Chem. Phys. 18 (2016) 8827-8839. https://doi.org/10.1039/C5CP06693J
6. H. Bloemendal, W. De Jong, R. Jaenicke, N.H. Lubsen, C. Slingsby, A. Tardieu, Ageing and vision: structure, stability and function of lens crystallins, Progress in Biophysics & Molecular Biology. 86 (2004) 407-485, https://doi.org/10.1016/j.pbiomolbio.2003.11.012